Chem Soc Rev

TUTORIAL REVIEW

View Article Online
View Journal | View Issue

Cite this: *Chem. Soc. Rev.*, 2020, **49**, 4667

Harnessing the surface structure to enable high-performance cathode materials for lithium-ion batteries

Luyi Yang,[a] Kai Yang,[a] Jiaxin Zheng,[a] Kang Xu,[b] Khalil Amine[c] and Feng Pan*[a]

Received 18th February 2020

DOI: 10.1039/d0cs00137f

rsc.li/chem-soc-rev

The ever-increasing demand for high-performance batteries has been driving the fundamental understanding of the crystal/surface structural and electrochemical properties of intercalation cathode materials, among which the olivine-type, spinel, and layered lithium transition metal oxide materials have received particular attention in the past decade due to their successful commercialization. While the most current studies focus on the macroscopic and bulk crystal structure of these materials, our previous work suggests that, as a confined region wherein charge transfer takes place, the electrochemical performances of the interfacial structures of cathode materials are largely dictated by the break in the structural symmetry from 3D (bulk) to 2D (surface), which leads to reconstructions under different chemical/electrochemical conditions. By summarizing various works in this subject and offering our perspectives, this tutorial review will reveal for the first time the correlation between the surface structure and interface reconstruction at atomic/molecular scales and their direct impact on the corresponding electrochemical performances. More importantly, by extending the knowledge obtained from these three well-studied system, we believe that the same established principles could universally apply to other cathode materials that have been the frontiers of new battery chemistries.

Key learning points

1. Poorly crystalline and disordered surfaces can be reconstructed for higher capacities.
2. Electrolyte solvents are found to reconstruct the cathode/electrolyte interface, thus tuning the ion transfer kinetics.
3. The depolarization of cathode materials can be achieved by a conductive coating layer that is in good contact with the cathode surface.
4. A chemically and electrochemically stable phase or coating layer could be artificially applied on the particle in order to prevent surface degradation.

Introduction

In the efforts to improve lithium ion batteries (LIBs), a high-performance cathode material is often the key bottleneck. Among all the reported cathode materials for LIBs, olivine-type $LiMPO_4$ (M = Fe, Mn, Co, and Ni), layered lithium transition metal (TM) oxide $LiTMO_2$ (TM = Ni, Mn, Co, or $Ni_xMn_yCo_z$, $x + y + z = 1$), and spinel $LiTM_2O_4$ (TM = Mn, Ti, Co, or V) represent the three major groups of intercalation structures, and have been adopted in diversified electric vehicles (EVs) around the world. The olivine-type cathode material was first reported by Goodenough and co-workers in 1997.[1] Among these, $LiFePO_4$ (LFP) is considered to be the most successful due to its moderate operating voltage (3.5 V *vs.* Li/Li^+), moderate capacity, excellent environmental friendliness, low cost, high abundance of Fe, and excellent stability and safety features. Layered lithium TM oxides present an alternative structural group to LFP with higher energy but lower safety and higher cost, whose application as automotive batteries is preferred given their longer driving range. Spinel Li_2MnO_4 (LMO), with abundant annual global production capacity, is also regarded to be attractive owing to its low cost and good rate capability, although its cycling instability has been a persistent issue.

Through periodic yet unique arrangement, basic structural units are able to constitute countless number of possible crystals.[2]

[a] *School of Advanced Materials, Peking University Shenzhen Graduate School, Shenzhen 518055, China. E-mail: panfeng@pkusz.edu.cn*
[b] *Energy Storage Branch, Sensor and Electron Devices Directorate, Power and Energy Division, US Army Research Laboratory, Adelphi, MD 20783, USA*
[c] *Electrochemical Technology Program, Chemical Sciences and Engineering Division, Argonne National Laboratory, Illinois 60439, USA*

These units can be considered as "material genes" that self-assemble into cathode materials and they generally dictate the charge transfer capability as well as the structural stability of the resultant materials.[2] For instance, the olivine structure of LFP (Fig. 1) consists of LiO_6 octahedra, FeO_6 octahedra, and PO_4 tetrahedra, wherein the Li-ion travels along the [010] direction. The strong covalent P–O bonding stabilizes O atoms and prevents oxygen release under oxidative conditions, thus making LFP a safe cathode material with excellent cycling stability.[3] In the charged (delithiated) state, Li-ions are removed to form the $FePO_4$ structure. This feature makes the lithiation/de-lithiation process of olivine LPF a two-phase transition reaction with a "transition zone" at the phase boundary, which differs from other cathode materials such as layered oxides. However, LFP exhibits relatively low electronic conductivity due to the covalent nature of its polyanions; meanwhile, the Li–Fe

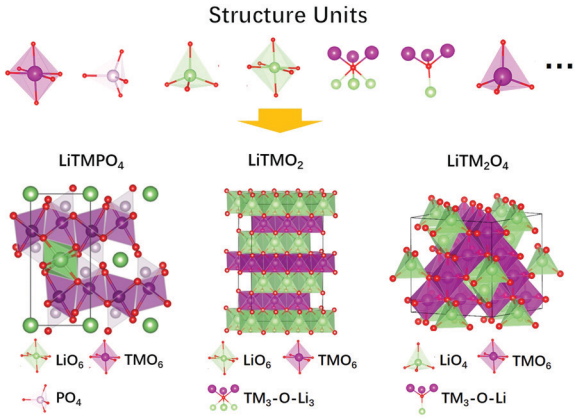

Fig. 1 The major structural groups of cathode materials (olivine $LiTMPO_4$, layered $LiTMO_2$, and spinel $LiTM_2O_4$) in LIBs.

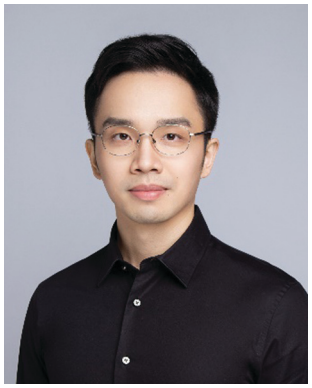

Luyi Yang

Dr Luyi Yang received his BS degree from the Department of Chemistry at Xiamen University (China) in 2010 and earned PhD degree from the School of Chemistry at Southampton University (UK) in 2015 under the supervision of Prof. John Owen. Dr Yang is currently a researcher at the School of Advanced Materials, Peking University, Shenzhen Graduate School. His research interests mainly focus on the investigation of key materials in lithium batteries including solid-state electrolytes, layered oxide cathode materials, and binders for Si anodes.

Kai Yang

Yang Kai is currently a PhD student in the School of Advanced Materials, Peking University, Shenzhen Graduate School under the supervision of Professor Feng Pan. He received his bachelor's degree from the School of Aerospace Engineering at Tsinghua University in 2016. His research focuses on the in situ advanced characterizations of interface issues in lithium batteries including in situ AFM, EQCM, DEMS, and other characterization tools from multi-scale dimensions.

Jiaxin Zheng

Jiaxin Zheng received his BSc in Physics in 2008 and PhD degree in Condensed Matter Physics in 2013 from Peking University, China. Then, he joined the group of Prof. Feng Pan at the School of Advanced Materials (SAM), Peking University, Shenzhen Graduate School, China, as a post-doctoral fellow from Oct. 2013 to Oct. 2015. Now, he works an Associate Professor (Principal Investigator) at SAM. His research interests include the discovery and tuning of functional structural units in cathode materials of lithium ion batteries, the extension of functional structural units to new battery materials, and the development of material genome methods.

Kang Xu

Dr Kang Xu is ARL Fellow and Team Leader at US Army Research Laboratory, adjunct professor at University of Maryland College Park, and co-founder of Center of Research on Extreme Batteries (CREB). With over 250+ publications and 6 book chapters, he is best known in the field for two comprehensive review articles on electrolytes published in Chem. Rev. (2004 and 2014). His work has been recognized by numerous awards, including 2017 IBA Technology Award, 2018 ECS Battery Research Award, and 2017 Scientist-of-the-Quarter in US DoD.

anti-site defects also result in poor percolation properties of the Li^+ diffusion channel, leading to sluggish Li^+ diffusion.[4] Magnetic order at the room temperature in Li_xFePO_4 ($x \leq 0.12$) was reported recently by Pan and co-workers,[5] who described that the magnetism originating from the Fe/Li anti-site defects creates Fe^{2+}–Fe^{3+} super-exchange to generate the strong Lorentz force that decreases Li-ions, thus causing capacity loss. Other phosphates such as $LiTMPO_4$ (TM = Mn, Co, or Ni) have also attracted researchers due to their higher voltage plateau (>4 V *vs.* Li/Li^+) compared with LFP. However, pristine $LiMnPO_4$ (LMP) suffers from the mismatched $LiMnPO_4/MnPO_4$ interface, even poorer electronic conductivity, and the notorious Jahn–Teller distortion in the charged state of $MnPO_4$, which causes the deformation of the MnO_6 octahedra and Mn dissolution, and the subsequent severe capacity fading. With much higher operating voltages, $LiNiPO_4$ (LNP, 5.1 V *vs.* Li/Li^+) and $LiCoPO_4$ (LCP, 4.8 V *vs.* Li/Li^+) were studied as potential high-energy-density alternatives but their high operating voltages set a barrier that no current electrolyte systems have overcome yet.

Adopting the classic α-$NaFeO_2$ type structure, layered TM oxides belong to the rhombohedral space group $R\bar{3}m$ with edge-sharing TMO_6 octahedra, and therefore exhibit alternating layers of Li^+ and TM ions bridged by oxygen atoms (Fig. 1). Unlike LFP wherein the Li-ion diffuses along a 1D channel, Li-slabs in TM oxide allow the 2D diffusion of Li-ions from one LiO_6 octahedral site to another within the (001) plane. Instead of two phases such as in LFP, layered TM oxides exhibit a single-phase solid solution during reversible lithiation/de-lithiation. More importantly, since Li-slabs and TM-slabs are merely connected by oxygen atoms, for the formation of TM_3–O–Li_3 oxygen structure units, layered TM oxides are less stable than LFP. One major issue faced by layered TM oxides is the Ni/Li disordering, wherein Ni occupies the 3b sites in the Li-slab and Li occupies the 3a sites in the TM-slab due to the similar radii of Li^+ and Ni^{2+}. A high degree of Li/Ni disorder generally leads to poor specific capacity and cycle life. Furthermore, side reactions between the layered TM oxides and the electrolytes, surface phase transformation, as well as particle cracking during repeated cycling could also contribute to capacity fading.[6] In recent years, Ni-rich layered oxides with high capacities have been intensively investigated, which are faced with not only more challenging storage and preparation issues but also with a less stable surface due to high Ni content.[7]

The crystal structure of $LiMn_2O_4$ exhibits the cubic spinel *Fd3m* space group with face-sharing 8a tetrahedral Li and 16d octahedral Mn (shown in Fig. 1, right). During Li^+ insertion, additional Li-ions can be stored in the 16c octahedral sites, which facilitate energetically accessible 3D interstitial pathways for Li^+ diffusion together with the 8a tetrahedral sites. The result of such a structural nature is the good rate capability of the spinel LMO. However, LMO intrinsically suffers from poor cycling stability.[8] On the one hand, the discharge process induces an Mn^{3+}-rich domain and causes Jahn–Teller distortion, further leading to Mn dissolution as well as blockage of the Li diffusion pathway. On the other hand, Li insertion also results in phase transition from cubic $LiMn_2O_4$ to tetragonal $Li_2Mn_2O_4$, accompanied by a large volume change and lattice mismatch, thus compromising the structural integrity.[8] In particular, LMO is especially susceptible to the attack of HF generated from water residue and $LiPF_6$ salt in the electrolyte, thus causing sustained surface degradation.

Although most efforts have focused on their bulk properties, it is noteworthy that as the confined region for the charge transfer process to occur, the interfacial structures have a tremendous impact on the electrochemical properties (*e.g.*, capacity, cycle life, and high-rate performance) of battery materials. However, since the interface between the cathode and the electrode is an area of very limited presence, its chemical and electrochemical

Khalil Amine

Dr Khalil Amine is a Distinguished Fellow and the Manager of the Advanced Battery Technology programs at Argonne National Laboratory, where he is responsible for directing the research and development of advanced materials and battery systems for HEV, PHEV, EV, satellite, military, and medical applications. Dr Amine currently serves as a member of the U.S. National Research Consul on battery related technologies. Dr Amine holds/has filed over 196 patents and patent applications and has over 608 publications. From 1998–2008, Dr Amine was the most cited scientist in the world in the field of battery technology.

Feng Pan

Prof. Feng Pan, Chair-Professor, Founding Dean of School of Advanced Materials, Peking University, Shenzhen Graduate School, Director of National Center of Electric Vehicle Power Battery and Materials for International Research, received his BS degree from the Dept. of Chemistry, Peking University in 1985 and PhD from Dept. of P&A Chemistry, University of Strathclyde, UK with "Patrick D. Ritchie Prize" for the best PhD in 1994. Prof. Pan has been engaged in fundamental research on structural chemistry, exploring "Material Gene" for Li-ion batteries, and developing novel energy conversion-storage materials and devices. He also received the 2018 ECS Battery Division Technology Award.

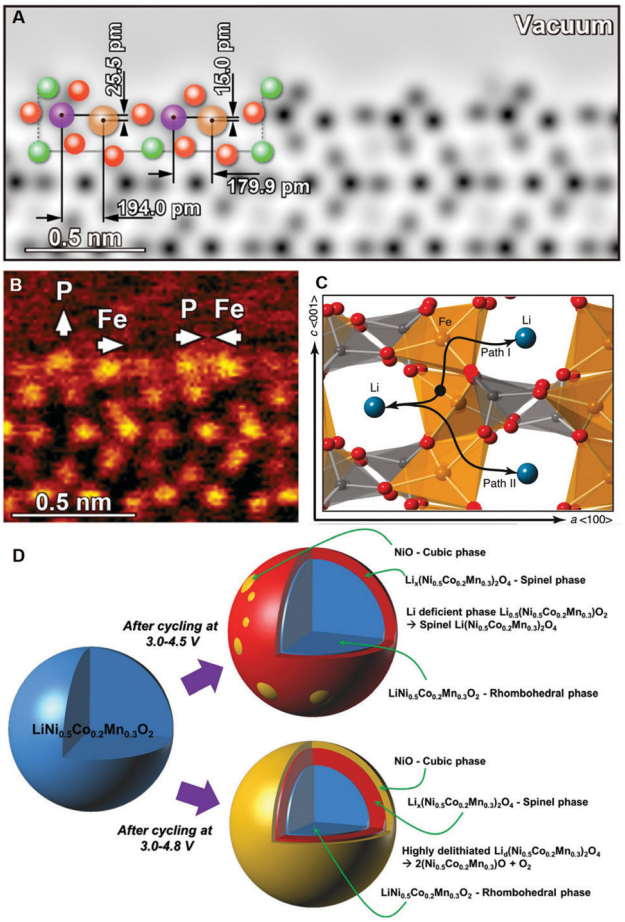

Fig. 2 (A) Simulated annular bright field scanning transmission electron microscopy (ABF-STEM) image, wherein different atoms are colour-coded: Li-green, Fe-brown, P-purple, O-orange; (B) magnified ABF-STEM colour images. The direction of atom shift is indicated by the white arrows. Reproduced from ref. 9 with permission from American Chemical Society, copyright 2016. (C) Li^+ diffusion pathways on the LFP surface. Reproduced from ref. 10 with permission from American Chemical Society, copyright 2011. (D) Proposed transformation mechanisms of NCM532. Reproduced from ref. 11 with permission from WILEY-VCH Verlag GmbH & Co. KGaA, Weinheim, copyright 2013.

information is often obscured by the bulk. For instance, due to the disappearance of the crystalline periodicity at the particle surface, the structural symmetry of the cathode material is suddenly reduced from 3D to 2D and such a discontinuity usually presents high barriers to mobile ions. Owing to the development of advanced computational methods as well as surface characterization techniques, a better understanding of the surface structures, interface reconstruction, and chemical properties in battery materials has been obtained in recent years. Kobayashi and co-workers used annular bright field (ABF) scanning transmission electron microscopy to examine the (010) surface of LFP.[9] As shown in Fig. 2A and B, they found that when the outer surface layer is shielded by Li atoms, P and Fe atoms have a larger vertical shift and larger distance, whereas, when the surface Li site is vacant, P and Fe move towards each other. However, after chemical de-lithiation, Li^+ ions are found to relax back to the bulk and the surface Li^+ ions cannot be recovered even after 3000 h of relaxation. Therefore, it could be inferred that the surface of the olivine material may undergo structural reconstruction during the electrochemical processes. In addition, according to density functional theory (DFT) calculations, the migration process of Li^+ across the LFP(010)/vacuum interface (Fig. 2C) constitutes the limiting step due to the high migration energy.[10]

The surface structures of layered TM oxides also dictate their electrochemical performance. It has been reported by Kang and co-workers that when $LiNi_{0.5}Co_{0.2}Mn_{0.3}$ (NCM523) is cycled under a cut-off voltage of 4.5 V, the capacity retention is much higher than that when it is cycled up to 4.8 V. This is because the surface of the particle undergoes a phase transformation from the rhombohedral phase to the spinel phase with a trace of the rock salt phase of NiO when cycled under 4.5 V (Fig. 2D). On increasing the cut-off voltage to 4.8 V, the formation of the rock salt phase is significantly accelerated under the highly oxidative environment, accompanied by rapid capacity fading.[11] However, such transformation is not observed in the $LiNi_{1/3}Co_{1/3}Mn_{1/3}$ (NCM111) material, which can be attributed to the lower content of Ni. In addition, the basic surface of NCM materials (especially for Ni-rich NMC) tends to react with CO_2 in air, thus forming Li_2CO_3 on the surface. It has been reported that impurities such as Li_2CO_3 could generate gas under high voltage, react with the electrolyte, and block Li^+ diffusion channels.[7]

Therefore, in order to optimize the electrochemical performance of cathode materials, a new interface is necessary through reconstruction reactions, which may vary with different chemical and electrochemical conditions. For instance, Ceder and co-workers reported that by forming a layer of fast ion-conducting amorphous phase on LFP through a controlled off-stoichiometric preparation method, ultrafast charging and discharging performance can be achieved.[12] More importantly, due to the relatively lower operating voltages and robust crystalline structures, undesirable side reactions (*e.g.*, Li/O release and electrolyte degradation) are less likely to occur on the LFP surface. Consequently, the surfaces of olivine and layered TM oxides represent two vastly different types of interfacial chemistry and electrochemistry.

In this tutorial review, as demonstrated in Fig. 3, four types of interface reconstructions, according to the surface structures of different LIBs cathode materials, will be summarized, which exhibit great relevance to the electrochemical performances including specific capacity, rate capability, and cycling stability. By reviewing the recent advances in this area, we aim to clarify some fundamental questions about the interfaces of not only olivine, spinel, and layered oxides but also other cathode materials in general: how do mobile ions behave at the interface where structural discontinuity occurs? Why is the interfacial structure so important to the bulk electrochemical performance? And how do we design to achieve a desirable interface?

Boosting capacity *via* surface modification

The achievement of high-rate performance in LFP generally requires reduced particle sizes for shorter Li-ion diffusion path.

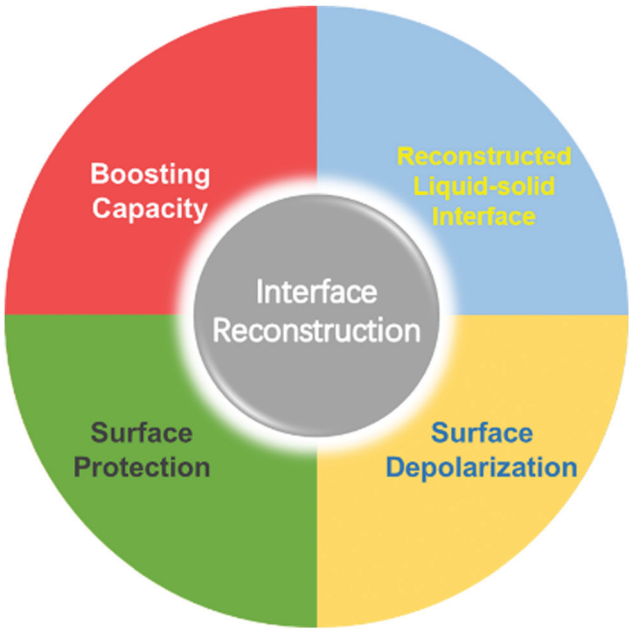

Fig. 3 Diversified types of surface/interface reconstruction for olivine cathode materials.

However, this approach could compromise the overall energy density on the device level by lowering the tap density. Moreover, the large surface area could also accelerate the side reactions such as transition metal dissolution and electrolyte decomposition. In order to take full advantage of nanosized olivine materials, one effective strategy is to utilize their large specific surface areas by creating extra Li^+ storage sites on the particle surface. In 2013, Li and co-workers proposed LFP modified by exfoliated graphene (EG) *via* van der Waals interaction,[13] which consists of a thin layer of graphene (1.5–2 nm) coated on LFP particles. Consequently, a specific capacity of 208 mA h g^{-1} was achieved, which surpassed the theoretical value of LFP (170 mA h g^{-1}). More importantly, Li^+ insertion into EG was also observed after discharge. The authors hence attribute the excess capacity to the reversible redox-based Li^+ storage due to the defects at the edge sites or the basal planes of the EG. In addition, the EG coating also promotes carrier mobility and reduces polarization.

Xiao and co-workers prepared a carbon encapsulated LFP (GC/LFP) with internal carbon (IC) sheet composite (GC/IC/LFP) using phytic acid.[14] Interestingly, both X-ray diffraction (XRD) and transmission electron microscopy (TEM) results indicate that compared with GC/LFP, GC/IC/LFP has a larger lattice parameter, which allows for faster Li^+ transfer. As a result, the obtained GC/IC/LFP exhibits a specific capacity of 192 mA h g^{-1}, which is also greater than the theoretical value of neat LFP. Both cyclic voltammograms and dQ/dV curves exhibit two redox peaks, suggesting that the excess capacity is related to an independent reversible redox reaction. It was speculated that the extra Li^+ might be stored both in the IC or its defects and edges. Alternatively, Sun and co-workers grew oxygen-containing functional groups (*e.g.*, N–O$^\bullet$ and C=O) on a carbon surface coated on LFP, resulting in a capacity of 190 mA h g^{-1}.[15] They believed that these functional groups grafted on the carbon surface can be reversibly oxidized and reduced during the charge and discharge processes, hence providing extra binding sites for Li^+.

Despite the excitement about excess Li storage on the surface, the microscopic mechanisms behind such a behaviour remained unclear. To have a better understanding of their origin, Pan and co-workers investigated the surface Li storage mechanism from the atomic perspective.[16] By creating C–O–Fe bonds between the thin carbon coating layer and LFP, a new composite LFP-E was obtained, which also exhibited an ultra-high capacity of 208 mA h g^{-1} (Fig. 4A). Combined with *ab initio* calculations, it can be observed (Fig. 4B) that due to the broken symmetry, Fe atoms on the surface of LFP are coordinated by 5 O atoms instead of 6, forming FeO_5 pentahedrons. This feature lowers the number of Li^+ storage sites on the surface by 50%. By compensating the truncated symmetry of the surface Fe atoms, the Fe–O–C bonds not only restored the original Li^+ storage sites but also create extra sites ($Li1_{LFP\text{-}E}$ and $Li2_{LFP\text{-}E}$) on the reconstructed surface by providing surface dangling O atoms that could bind with Li^+. It is noteworthy that the excess capacity is also size-dependent. Fig. 4C summarizes the theoretical and experimental size-dependence of the specific capacity for LFP. Since smaller particles possess higher reconstructed surface areas and more excessive binding sites, higher capacity can be obtained thereon. In addition, this method was also effective on other olivine composites such as LMP, LCP, $LiFe_{0.5}Mn_{0.5}POI_4$, and $LiFe_{0.5}Co_{0.5}PO_4$. By modifying the surface crystalline defects on olivine cathode materials, this approach opens up a new opportunity for improving the capacities.[16]

Liu and co-workers also carried out first-principles total energy calculations on the Li insertion behaviour at the lithium manganese iron phosphate (LMFP)/graphene interface,[17] which allows the storage of 8 Li atoms with an insertion energy (E_{ins}) lower than 2 eV, corresponding to the lower cut-off voltage of 2.0 V (Fig. 5). According to this result, an excess capacity of

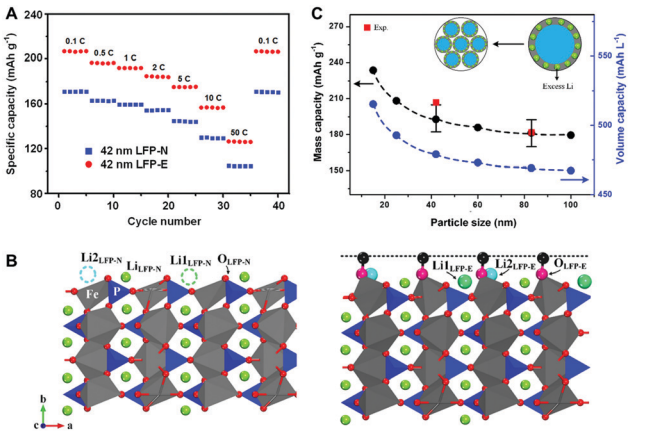

Fig. 4 (A) Rate capabilities of LFP-N and LFP-E; (B) lithium and electron transfer sites of excess Li atoms in LFP-N (left) and LFP-E (right); (C) experimental and theoretical size-dependent excess capacity in LFP. Reproduced from ref. 16 with permission from American Chemical Society, copyright 2017.

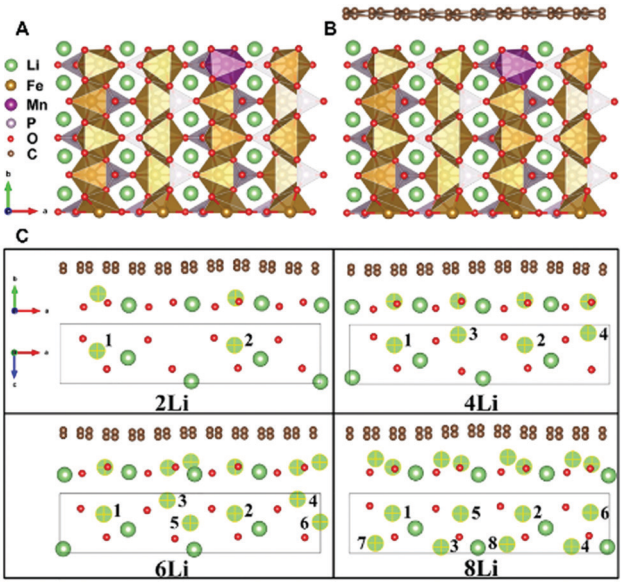

Fig. 5 Side views of the structures of (A) the LMFP surface and (B) the graphene/LMFP interface. (C) Top and side views of the geometry optimized G/LFP interface with different numbers of inserted Li atoms. Only the outermost Li and O atomic layers are presented. Li atoms inserted are marked with yellow cross. Reproduced from ref. 17 with permission from Elsevier, copyright 2017.

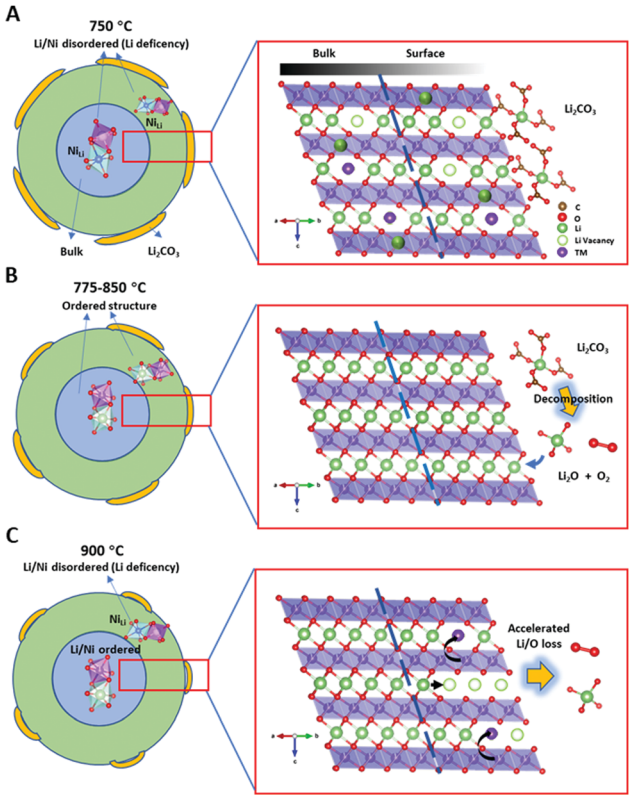

Fig. 6 Schematic illustrations of how the cationic ordering is coupled to the surface reconstruction of NMC71515 under different sintering temperatures. Reproduced from ref. 18 with permission from Royal Society of Chemistry, copyright 2019.

0.36 mA h cm^{-2} (per specific surface area of the LFP particles) could be contributed by such an interface, which is in agreement with the previous conclusion that the excess capacity is largely dependent on the particle size of the olivine cathode material.

For lithium TM oxides, the more pressing issue is to suppress the formation of electrochemically inactive species on the surface. It is known that the sintering temperature of $LiNi_{0.7}Co_{0.15}Mn_{0.15}O_2$ (NCM71515) plays a critical role in its electrochemical performances.[18] On the one hand, when the temperature is too low, Li_2CO_3 formed on the surface barely decomposes, leading to a Li-deficient particle surface with a passivation layer, and hence, the low capacity (Fig. 6). On the other hand, if the temperature is too high, while it is sufficient for the structural ordering process, the rate of Li/O loss at the surface is promoted, leading to a Li-deficient phase near the particle surface. Therefore, by choosing an optimized temperature window, desirable surface reconstruction (Li_2CO_3 decomposition) could be favoured while unwanted Li/O loss could be circumvented. More recently, it has also been found that cooling-induced surface reconstruction has a pronounced effect on the capacity as well as the rate capability.[19] By adopting a quenching process, the accumulation of Li_2CO_3 on the surface is suppressed; hence, the Li-deficient phase on the surface can be effectively avoided.

Pan and co-workers proposed a pre-lithiation process to improve the capacity and cycling stability of the $LiNi_{0.5}Co_{0.2}Mn_{0.3}O_2$ (NCM523) material by treating the active material at a low voltage (1.2 V *vs.* Li/Li^+) before cycling.[20] As a result, an SEI due to electrolyte reduction can be formed on the particle surface of NCM523, which prevents Mn^{2+} dissolution during subsequent cycling in normal voltage ranges. More importantly, an additional layer of Li^+ can be reversibly stored in the surface, thus contributing to a higher capacity (Fig. 7).

Reconstructing the liquid–solid interface

The diffusion of Li^+ across the interface is more sluggish than in the bulk; hence, the approach to accelerate this process is of high significance. According to Bazant and co-workers, *ab initio* molecular dynamic (MD) simulations show that Li^+ transfer

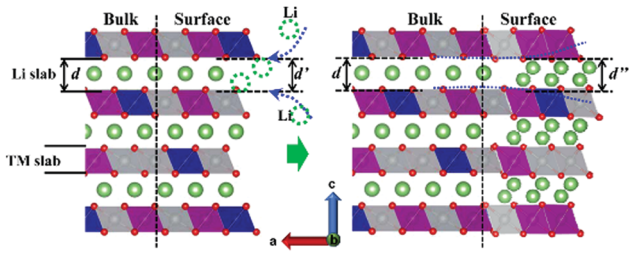

Fig. 7 Schematic mechanisms of the pre-lithiation process for NCM523. Reproduced from ref. 20 with permission from American Chemical Society, copyright 2015.

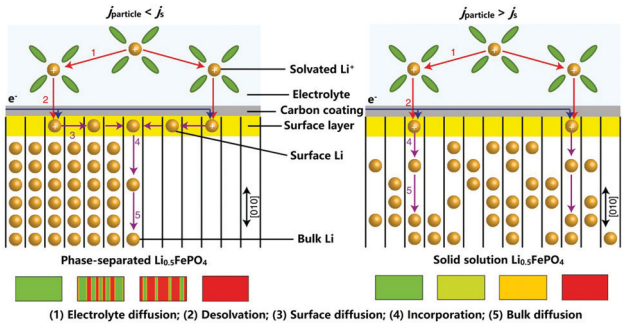

Fig. 8 Different Li^+ diffusion mechanisms during phase separation (left) and solid solution reaction (right). Reproduced from ref. 21 with permission from Nature Publishing Group, copyright 2018.

between the LFP (010) face and vacuum is inhibited due to the high diffusion energy.[21] The presence of both organic and aqueous solvent molecules is found to assist this surface diffusion, rendering LFP a 3D Li^+ conductor (Fig. 8). Therefore, understanding the Li^+ migration mechanism at the interface between olivine materials and the electrolyte at molecular/atomic scales becomes critical for designing and developing materials.

In recent years, aqueous electrolytes have attracted extensive interests due to their intrinsic safety and lower costs than conventional non-aqueous electrolytes. Due to the relatively low operation potential of LFP, aqueous electrolytes can stably support such a cathode without generating oxygen at its anodic limits. Using nanosized LFP as the cathode material, Pan and co-workers compared the electrochemical performance of an aqueous electrolyte with 0.5 M Li_2SO_4 with a conventional carbonate electrolyte.[22] The water-based electrolyte exhibited ultrafast rate capability (72 mA h g^{-1} at 600C, corresponding to 42% charge completed at 6 seconds), which is much higher than that of the carbonate (20 mA h g^{-1} @ 200C). Using DFT simulation, it is proposed that this difference originated from a "Janus interface" facilitated by H_2O molecules. The FeO_6 and LiO_6 octahedral structure units in the crystal experience a break in the symmetry to become FeO_5 and LiO_3 units at the surface (Fig. 9A), which can be compensated by O atoms from H_2O, thus forming $FeO_5(H_2O)$ and $LiO_3(H_2O)_3$ octahedra; meanwhile, H atoms could also form strong hydrogen bonds with adjacent O atoms to widen the Li^+ passage by approximately 0.2 Å for faster Li^+ (de)intercalation. Consequently, a transition structure that resembles both the solid and liquid phases is formed, which serves as the optimum transition phase for fast Li^+ transfer. In addition, for the aqueous electrolyte, the overall energy barrier of the de-solvation process is much lower than that in the organic electrolyte due to the fewer number of H_2O molecules involved (Fig. 9B and C).

To further understand the underlying mechanisms, advanced electrochemical characterization techniques have been tailor-made and employed. For instance, by using an electrochemical quartz crystal microbalance (EQCM), Pan and co-workers measured the mass changes in LFP and NFP cathode during electrochemical processes.[23] In the organic electrolyte, LFP exhibits

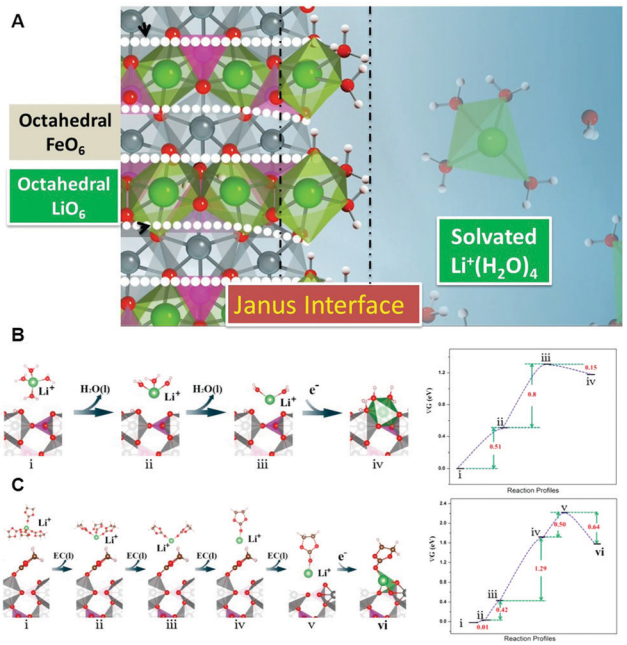

Fig. 9 (A) Proposed Janus solid–liquid interface between LFP and the aqueous electrolyte; reaction profiles for Li-ion transport across the $FePO_4/H_2O$ interface (B) and $FePO_4$/ethylene carbonate (EC) interface (C) in the discharge process and their energies at each step (right-hand panels). Li, green; Fe, grey; P, purple; O, red; C, brown; H, white. Reproduced from ref. 22 with permission from American Chemical Society, copyright 2015.

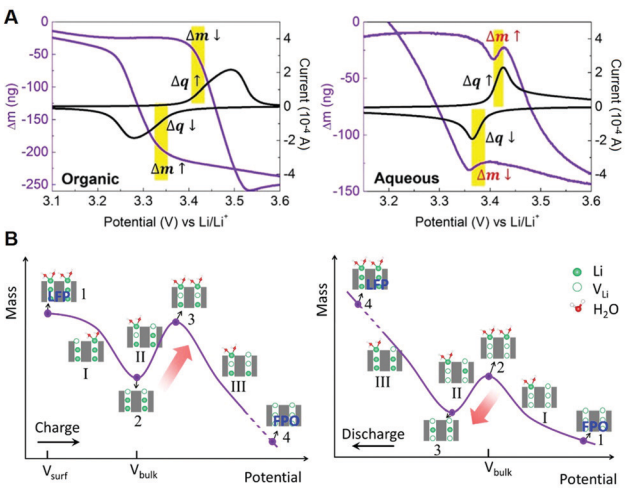

Fig. 10 (A) Mass–potential curves (purple line) and CV curves (black line) of LFP in the organic electrolyte (left) and the aqueous electrolyte (right); (B) proposed mass–potential curves for $LiFePO_4$ in the aqueous system during charge (left) and discharge (right). Reproduced from ref. 23 with permission from Elsevier, copyright 2017.

conventional Li^+ (de)intercalation processes as expected (Fig. 10A); however, in the aqueous electrolyte, the mass curve shows an increasing trend in the range of 3.42–3.44 V *vs.* Li/Li^+ even during charging and a similar anomalous mass change interval can also be observed during cathodic scanning. The mass–charge curve obtained from the aqueous solution shows

a higher value of 11 g mol^{-1} compared to that in the organic electrolyte (approximately 7 g mol^{-1}, equivalent to the mass/charge ratio of a Li^+). The intercalation/deintercalation processes can be divided into two stages (Fig. 10B): during the surface redox process, H_2O molecules are desorbed with surface Li^+ when the potential reaches the de-lithiation "surface potential" (V_{surf}), at which the bulk Li^+ have insufficient driving force to migrate into the surface layers due to V_{surf} (2.9 V) < V_{bulk} (3.4 V), according to the DFT calculation. Then, the H_2O molecules are re-adsorbed on Li^+ of the LFP surface once the potential is raised to V_{bulk}, whereas during the bulk redox process, the surface reaction reaches a dynamic equilibrium, leading to a continuous mass change. In contrast, such a behaviour cannot be observed in an aqueous NFP cell, which can be ascribed to the fact that the surface and bulk redox voltages are too close to distinguish under the conditions of the cyclic voltammetry (CV) measurement. Interestingly, it has also been reported that unlike the non-aqueous electrolyte, Na^+ can be preferentially inserted into the $FePO_4$ framework over Li^+ in the aqueous solution due to the lower energy barrier at the $FePO_4/H_2O$ interface.[24] Taking advantage of this feature, NFP with good electrochemical performance can be synthesized *via* a facile ion-exchange process.

Thick electrodes with high areal loading and particle aggregation are favoured in consideration of their high energy densities. As a result, too much information (*e.g.*, particle–particle interaction, pore-accessibility by the electrolyte, and concentration polarization within the electrolyte) is entangled in the electrochemical data obtained, which cannot reflect the intrinsic properties of individual single particles. In addition, galvanostatic intermittent titration technique (GITT) is not suitable for LFP due to its flat voltage plateaus. To exclude these interfering factors and to obtain the electrochemical information of single LFP particles, Pan and co-workers fabricated an ultrathin single-particle (SP) electrode,[25] wherein the LFP nanoparticles were uniformly scattered within the conductive network. Compared with the conventionally prepared electrode (thick electrode), the anodic peak for the SP electrode shows a much narrower half-width (Fig. 11A), indicating minimized polarization effect. A novel SP Model was then developed to fit the CV curves of the SP electrodes, which include the Li^+ diffusion process and the interface charge transfer process to obtain the parameters of Li^+ diffusion coefficients (D_{Li}) and interface reaction rate constants (K_0). It can be seen from Fig. 11B that the CV curves of the SP electrodes in both water-based and carbonate electrolytes can be well fitted by the model. The fitted K^0 in the aqueous electrolyte is higher than that in the organic electrolyte by one order of magnitude. Herein, the K^0 value is associated with the pre-exponential factor (A) and activation energy (E_a) ($\ln K_0 = \ln A - E_a/RT$; R: molar gas constant; T: thermodynamic temperature), while A and E_a can be attributed to the de-solvation (solvation) process and interface reconstruction with the solvent (*e.g.*, H_2O–Fe coordination), respectively (presented as Step II in Fig. 11C). This result agrees with the previous conclusion that the de-solvation process is the determining step for Li-ion transport across the $FePO_4$/electrolyte interface. Recently, the

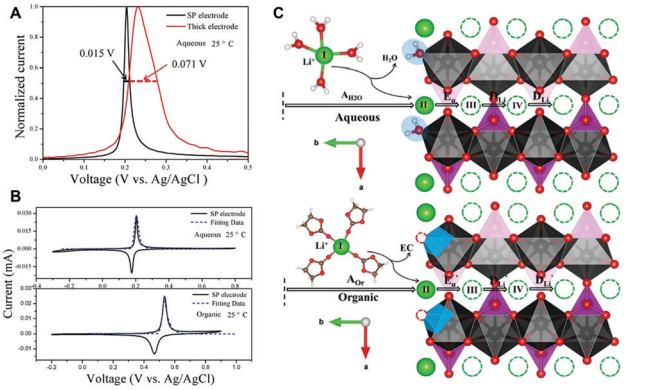

Fig. 11 (A) CV curves of the SP and thick electrodes; (B) CV curves of the SP electrode and the thick electrode in aqueous and organic electrolytes at 25 °C with the current density of 1 mV s^{-1}; the dotted lines are the simulation curves by the SP-model; (C) the interfacial reaction profiles for Li-ion transport across the $FePO_4/H_2O$ interface and $FePO_4$/EC interface in the discharge process. Reproduced from ref. 25 with permission from WILEY-VCH Verlag GmbH & Co. KGaA, Weinheim, copyright 2016.

effect of anion adsorption layer on the inner Helmholtz plane was also investigated. It was revealed that different anions exhibit different binding energy with the LFP surface, resulting in a significant impact on K_0 and E_a.[26]

Surface doping is also found to have a significant impact on the reconstruction of the solid–liquid interface. Chen's group reported that by doping a small amount of Ni on the surface of LMO, the capacity and rate performance of LMO is greatly promoted at −20 °C.[27] Through DFT calculations, it is revealed that the reconstructed interface demonstrates a significantly reduced energy barrier for charge transfer and Li binding energy. Therefore, the synergistic effect in the outermost layers lowers the threshold energy of the interfacial reactions. It should be noted that owing to the unstable electrode–electrolyte interface during cycling, it is much more difficult to obtain detailed interfacial information about the spinels and the layer oxides. For future studies, one key challenge is to optimize the testing conditions.

Depolarizing cathode materials and electrodes

The slow Li^+ diffusion and poor intrinsic electronic conductivity have imposed severe restrictions on the rate performances of cathode materials; therefore, several measures have been adopted to address this issue. The surface/interface depolarization of cathode materials can be carried out by either improving the ionic or the electronic conductivities. With the aid of a statistical method of Tafel analysis, Bai and Bazant reveal that electron transfer at the solid–solid interface constitutes the limiting step in the reaction kinetics of LFP rather than the ion transfer at the liquid–solid interface.[28]

The most commonly used strategy for obtaining higher electronic conductivity is to coat a thin layer of a conductive material (*e.g.*, carbon) on the surface of olivine materials.

Generally, the carbon coating process involves the pyrolysis of organic precursors in a reducing atmosphere. As shown in Fig. 12A, an LFP/C nanocomposite material was synthesized by a self-regulated *in situ* polymerization method (Step I), followed by a rapid Li^+/H^+ ion exchange step (Step II) and calcination (Step III).[29] On the one hand, LFP/C particles with highly crystalline LFP cores were obtained; on the other hand, highly graphitized carbon was formed on the LFP surface due to the catalytic effect of Fe^{3+}. This ideal feature can be attributed to the hybrid structure of the Li–$FePO_4$/PFA intermediate with a well-closed polymer "shell" and a homogeneous "core", wherein essential elements are homogeneously distributed at the atomic level. This LFP/C composite obtained from such a method (PrepLFP) exhibits superior rate capacity (Fig. 12B) as well as power/energy density (Fig. 12C) compared with other battery/supercapacitor materials.

The choice of a conductive additive also determines the electronic conductivity. Pan and co-workers compared the effect of carbon with different contacting properties on the performance of LFP cathodes.[30] They found that soft-contact carbon (SCC) with a less crystalline structure enables better electronic conduction as compared with hard-contact carbon (HCC), thus leading to superior rate capability. SCC induces plane-like contact with a large area rather than the point-like contact generated by HCC, according to the simulation (Fig. 13). More uniform current density vectors are expected for the interface between LFP and SCC, hence alleviating the polarization effect.

However, it should be noted that the carbon coating can cause non-stoichiometric composition on the LFP surfaces, leading to unwanted capacity loss. It has been reported by Sun and co-workers that during the carbon-coating process, electrochemically inert phases (Fe_2P and $Fe_2P_2O_7$) emerge on the surface due to lithium loss during thermal treatment. Moreover, the formation of these impurity phases is highly

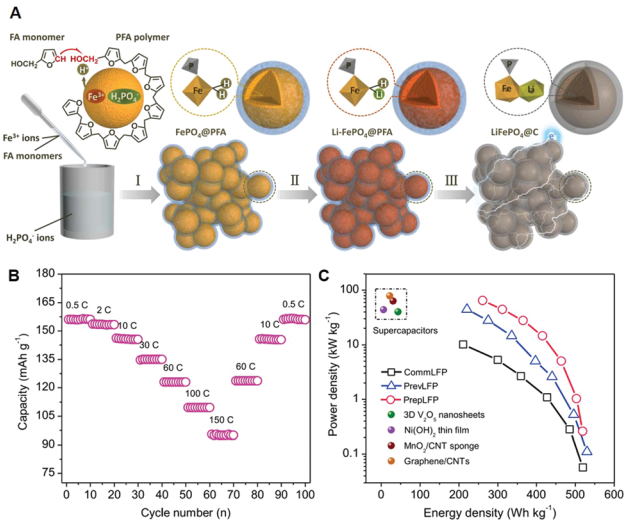

Fig. 12 (A) Schematic illustration for the preparation process of the LFP/C material; (B) rate performance and (C) Ragone plot of power density *versus* energy density of the LFP/C nanocomposite. Reproduced from ref. 29 with permission from Elsevier, copyright 2017.

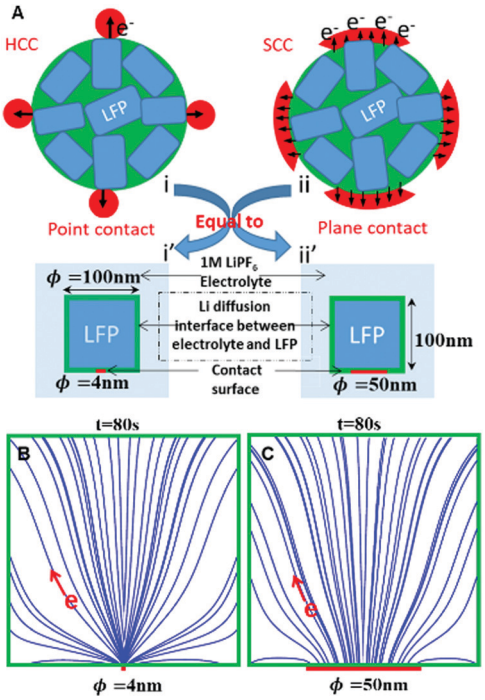

Fig. 13 (A) Schematic illustration of different contact types of LFP with HCC and SCC; simulated current density vectors within LFP for electrodes with (B) HCC and (C) SCC. Reproduced from ref. 30 with permission from Elsevier, copyright 2016.

dependent on the particle size, sintering temperatures, and the atmosphere.[31] Therefore, conductive polymers are also considered as promising coating materials for olivine cathode materials due to their environmental friendliness and low energy costs. Lepage *et al.* coated LFP particles with a thin layer of poly(3,4-ethylenedioxythiophene) (PEDOT) *via* the polymerization of 3,4-ethylenedioxythiophene (EDOT),[32] which resulted in excellent rate performance comparable to that of carbon-coated materials. Alternatively, Peng and co-workers proposed a conducting polymer coating of polyphenylene that binds with micron-sized LFP particles (about 1.01 μm) *via* a green diazonium chemistry (Fig. 14A),[33] in which the diazonium cations are first chemically reduced to phenyl radicals by LFP. DFT simulation results have shown that phenyl radicals could form strong chemical bonds with the O sites on a Li-deficient surface (Fig. 14B–D), which allows intimate binding between LFP and the conductive polymer. As a result, micron-sized LFP materials with improved electronic conductivity can be obtained, which exhibit excellent electrochemical performance.

Depolarization can also be achieved by surface doping. Goodenough and co-workers have reported that by doping nitrogen and sulphur on the surface of LFP, the rate capability can be greatly improved.[34] The calculation results show that nitrogen preferably substitutes for oxygen in the PO_4 tetrahedral and sulphur bonds to the undercoordinated Fe atoms on the surface (Fig. 15). As a result, the broken symmetry on the LFP surface is compensated. From the calculated binding energy of Li^+ as it diffuses from the (010) surface to different

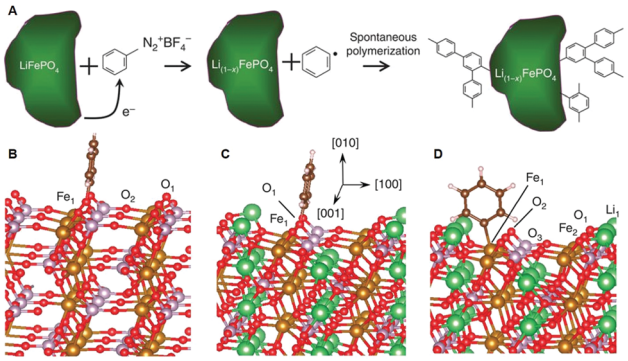

Fig. 14 (A) Schematic illustration of the polymerization reaction; DFT calculated configurations of the phenyl radical on the (010) face for (B) $FePO_4$, (C) LFP with Li vacancy, and (D) stoichiometric LFP. Reproduced from ref. 33 with permission from Nature Publishing Group, copyright 2015.

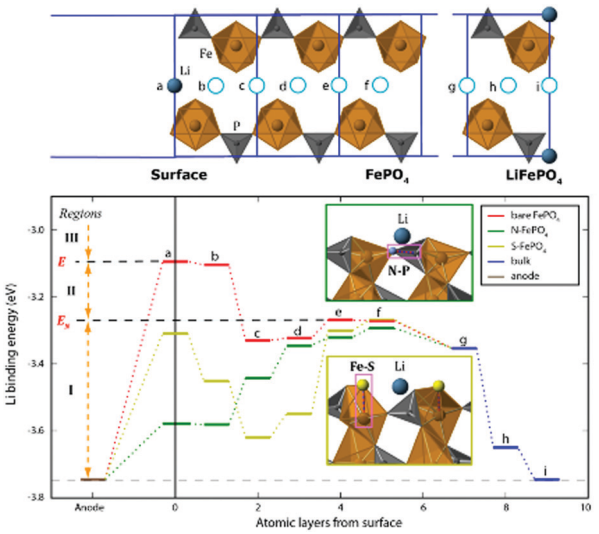

Fig. 15 Energy landscapes of Li moving through the surface of bare $FePO_4$ and doped $FePO_4$. Reproduced from ref. 34 with permission from American Chemical Society, copyright 2012.

atomic layers during the discharge process, it can be observed that on bare LFP, Li^+ binds weakly at the subsurface sites (a and b) owing to the undercoordinated surface. This binding becomes stronger as Li^+ reaches the bulk. The doping of N and S could effectively tune the energy levels on the surface by providing an empty state in the band gap and stabilizing the surface Fe 3d antibonding states, respectively, resulting in lower diffusion barriers for Li^+ diffusion. Alternatively, 1% Zr doping in Li-excess LFP ($L_{1.035}Zr_{0.01}FP$) is found to form a highly conductive layer on the surface,[35] which works synergistically with the carbon layer to enhance the conductivity. Consequently, improved rate performance was obtained. However, it should be noted that excessive doping (2% of Zr) inflicts a detrimental effect on the electrochemical performance due to the compromised LFP crystalline structures.

Since the carbon-coating technique requires a reducing atmosphere, which cannot be applied to layered lithium TM

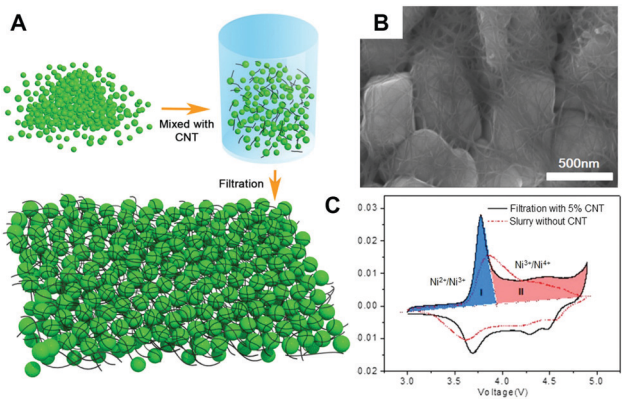

Fig. 16 (A) The schematic of the preparation process for the NCM/CNT film cathode; (B) scanning electron microscopy (SEM) image of the NCM/CNT cathode composite; (C) CV curve comparison for the slurry NCM without (dash line) and filtration NCM with CNT (solid line) cathodes. The two de-lithiation stages in the filtration NCM cathode are coloured in blue (I, Ni^{2+}/Ni^{3+}) and pink (II, Ni^{3+}/Ni^{4+}). Reproduced from ref. 36 with permission from American Chemical Society, copyright 2014.

oxides, building an electronic conductive network in such a system is more challenging. In order to address this issue, Pan and co-workers proposed a new concept of material design by embedding NCM523 particles in the single-walled carbon nanotube (CNT) network (Fig. 16A).[36] From Fig. 16B, it can be observed that the cathode particles are homogeneously wrapped by the CNTs, which serve as a highway for electron transfer, thus leading to a reduced electronic resistivity. As a result, the CV curve (Fig. 16C) of the NCM523/CNT composite shows a sharp peak indicative of fast kinetics.

Surface protection of cathode materials

Aurbach and co-workers proposed that the formation of trace HF, which is inevitable in the commonly used $LiPF_6$-based electrolytes, accelerates the failure of the LFP cathode.[37] On the one hand, Fe-ion experiences ion-exchange with H^+, causing Fe dissolution as well as capacity fading; on the other hand, Li^+ combines with F^-, forming highly resistive LiF, which slows down the charge transfer kinetics. Sun and co-workers later carried out the visual observation of the surface corrosion of LFP, wherein two types of impurity phases were identified: Fe-rich and P-rich phases.[38] It was found that severe Fe dissolution occurs in the Fe-rich phase due to the lower corrosion potential, which inhibits the corrosion of the adjacent area. On the contrary, the P-rich phase is more stable due to its high corrosion potential, which promotes the corrosion of the adjacent area. Despite these studies regarding the surface degradation mechanisms of LFP, its surface protection strategy has not been considered a priority owing to its excellent cycling stability.

Mn dissolution in LMP (same applies to LMO) is believed to have undergone a similar route, wherein the surface Mn is attacked by trace HF in the fluorine-containing electrolyte.

However, Mn dissolution is much more severe due to the instability of Mn^{3+}. More importantly, the dissolved Mn species are found to deposit on the anode (*e.g.*, graphite), thus causing further deterioration of the SEI and consumption of Li^+, consequently resulting in faster capacity fading.[39,40] Therefore, for the commercialization of Mn-doped olivine cathode materials, it is of great importance to suppress the dissolution of Mn species. It is increasingly clear and widely demonstrated that one of the most effective strategies is to apply a coating layer to stabilize the surface. In this case, how well-bonded the interface is between the coating layer and the cathode surface should also be taken into consideration. Huang and co-workers reported that by adding a small amount of bridging ions (*e.g.*, Fe and Co) during the coating process, strong bonding between the spinel and the coating agent (*i.e.*, Li_3PO_4) can be achieved.[41] They found that Fe and Co will diffuse into both the 16c sites to form a reconstructed interface (spinel–Fe(Co)–Li_3PO_4), which allows facile and homogeneous coating (Fig. 17). By contrast, in the absence of bridging agents, the same procedure does not result in a Li_3PO_4 coating layer on the surface.

For layered oxides, especially Ni-rich materials, side reactions on the liquid–solid interface could also lead to phase transition, and hence, the intergranular cracking. The electrolyte will then further infiltrate into the grain boundaries to react with the cathode materials. Therefore, a protective buffer layer could be effective in stabilizing the particle surface. Using the ALD technique, Yan *et al.* infused a solid electrolyte, Li_3PO_4 (LPO), into the grain boundaries of the Ni-rich layered oxide $LiNi_{0.76}Co_{0.14}Mn_{0.1}O_2$ material.[42] The LPO not only provides Li^+ diffusion pathways between the grain boundaries but also solidifies the grain boundaries of $LiNi_{0.76}Co_{0.14}Mn_{0.1}O_2$.

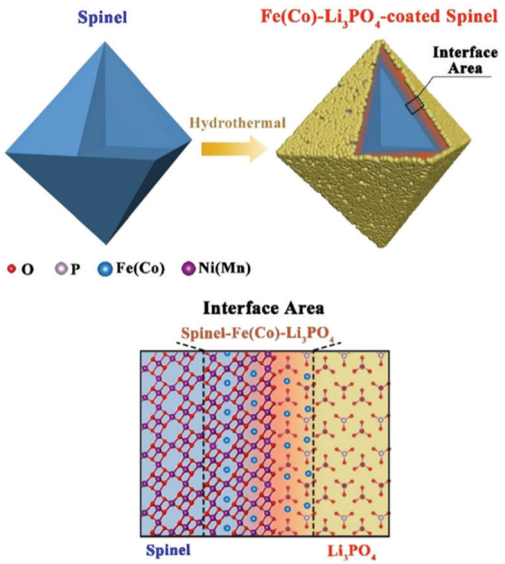

Fig. 17 Scheme of the phosphate coating mechanism of spinel cathode materials. The Fe and Co ions in the starting solution will migrate into the 16c sites of the spinel surface to form a bridged layer at the interface between the spinel and $LiPO_4$, thus facilitating a dense and uniform Li_3PO_4 coating layer. Reproduced from ref. 41 with permission from American Chemical Society, copyright 2019.

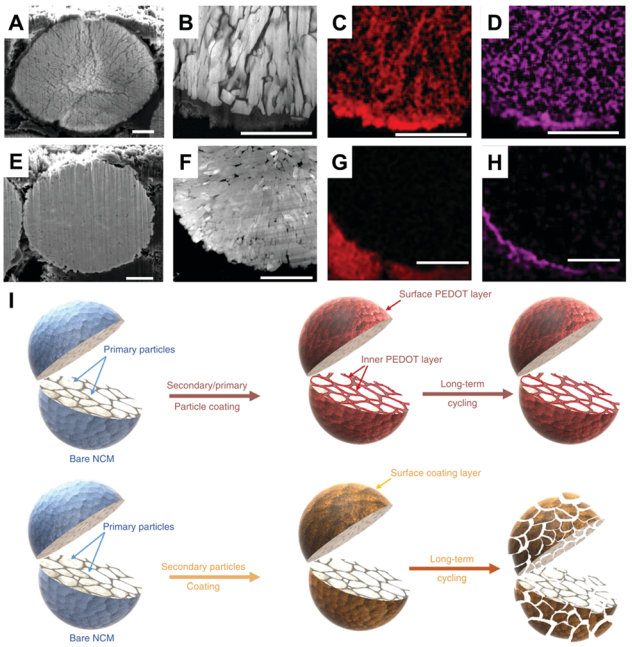

Fig. 18 Cross-sectional SEM image (A), scanning transmission electron microscopy high-angle annular dark field (STEM-HAADF) image (B), and the corresponding C (C) and F (D) maps of the pristine electrode after 200 cycles; cross-sectional SEM image (E), STEM-HAADF image (F), and the corresponding C (G) and F (H) maps of the LPO-infused electrode material after 200 cycles. Scale bars, 2 μm. Reproduced from ref. 42 with permission from Nature Publishing Group, copyright 2018. (I) An illustration of the structural stability of both the secondary/primary particle coating and the secondary particle coating only after long-term cycling. Reproduced from ref. 43 with permission from Nature Publishing Group, copyright 2019.

As a result, compared with the pristine material wherein severe intergranular cracking occurs during continuous cycling (Fig. 18A–D), the permeation of the liquid electrolyte is minimized by the LPO coating layer, thus suppressing the formation of the spinel-phase surface. As a result, the cracking is effectively prevented (Fig. 18E–H), hence leading to better electrochemical performances.

More recently, using oxidative chemical vapour deposition technique, Amine and co-workers applied a conformal coating of conductive poly(3,4-ethylenedioxythiophene) (PEDOT) polymer on both primary and secondary particles of layered oxide materials as the protective skin (Fig. 18I).[43] During long-term cycling, the PEDOT coating greatly enhances the phase and morphological stability of the layered oxides, exhibiting much higher capacity retention compared with bare particles. In addition, the PEDOT layer serves as an HF-scavenging agent by forming O–H–F bonds. As a result, the overall concentration of HF is decreased by 50% and TM dissolution is significantly inhibited, hence leading to better cycle stability.

An alternative approach to avoid the side reactions at the electrode/electrolyte interface is through the surface enrichment of a certain stable component. Liu and co-workers developed a concentration-gradient $LiMn_{0.8}Fe_{0.2}PO_4$ material (CG-LMFP).[44] Both X-ray photoelectron spectroscopy (XPS) and energy dispersive X-ray spectroscopy (EDXS) mapping analysis results

confirmed that CG-LMFP has a Fe-rich surface and an Mn-rich core. The obtained product shows remarkably enhanced stability against HF attack and effectively suppresses Mn dissolution. Superior cycling capacity and stability were achieved compared to pristine LMFP. Since lithium TM oxides (especially those rich in Ni) suffer from severe side reactions with the electrolyte at high voltages due to the instability of Ni^{4+}, diluting the Ni concentration on the surface is considered to be an effective method. Sun and Amine designed $LiNi_{0.75}Co_{0.1}Mn_{0.15}O_2$ with concentration-gradient nanostructures (Ni-rich core and Mn-rich surface).[45] The concentration of Co and Ni decreases linearly from the centre to the surface whereas Mn is enriched on the surface. This concentration-gradient material shows not only longer cycling life but also improved thermal stability. A Ti gradient doped (Ti/TM = 1.6%) $LiNi_{0.8}Co_{0.2}O_2$ (NC82) with high Ti concentration on the surface was developed by Pan and co-workers recently. Consequently, an electrochemically favoured disordered layered phase was formed at the surface, leading to a greatly improved cycling stability and superior rate capability. First-principles calculations further reveal that excellent electrochemical performance is attributed to the robustness of the oxygen-framework after Ti doping.[46] Similarly, Hu and co-workers synthesized spherical concentration-gradient $LiMn_{1.87}Ni_{0.13}O_4$, wherein the outermost layer is $LiMn_{1.5}Ni0_{0.5}O_4$ and the core is pure LMO.[47] Compared with pristine LMO, the concentration-gradient material delivers a much longer cycle life at elevated temperature (55 °C) as well as high operating voltage (3.0–4.9 V *vs.* Li/Li^+).

Alternatively, Oh *et al.* synthesized micron-sized $LiMn_{0.85}Fe_{0.15}PO_4$ coated with a layer of LFP with a thickness of 0.5 μm (Fig. 19).[48] This material not only adopts the high volumetric energy density of LMFP but also exhibits improved rate capability and cycling stability of LFP located at its outermost layer. A similar strategy was applied to $LiCoPO_4$ (LCP), which suffers from even more severe surface degradation owing to its high operation potential (~4.7 V). A robust monolithic LFP coat layer was hence formed by Manthiram and co-workers on high voltage vanadium-substituted LCP ($LiCo_{1-3x/2}V_x\square_{x/2}PO_4$) using microwave-assisted solvothermal approach.[49] Such LFP-coated LCP material exhibits lowered voltage polarization as well as the desired charge potentials. A coulombic efficiency of 100% can be achieved at x = 0.04, indicating mitigated surface side reactions. This surface protection approach can be universally applied to other materials. Through elegant atomic-level engineering, Pan and co-workers managed to design and synthesize a core–shell NCM@LFP material with aligned Li^+ tunnels, the result of which is the improved cycling stability of layered oxide materials at 4.6 V *vs.* Li/Li^+.[50]

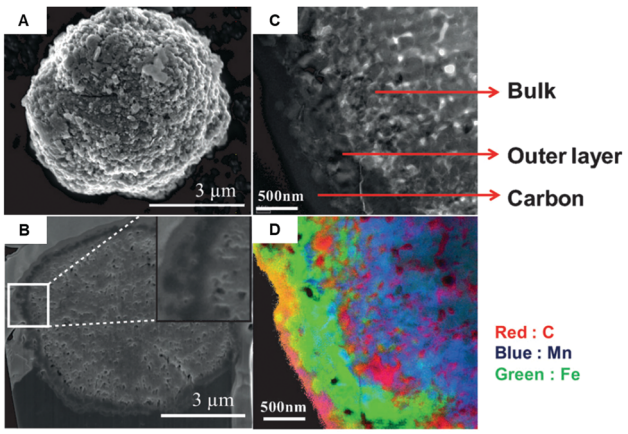

Fig. 19 SEM images of (A) double-structured $LiMn_{0.85}Fe_{0.15}PO_4$ LFP and (B) its cross-sectional image; (C) magnified cross-sectional TEM image and (D) its corresponding electron energy loss spectroscopy (EELS) image. Reproduced from ref. 48 with permission from WILEY-VCH Verlag GmbH & Co. KGaA, Weinheim, copyright 2012.

Conclusions

The recent advances in developing and understanding intercalation cathode materials have revealed the essential but overlooked role of the interfacial structure and chemistry in determining the electrochemistry of these materials. As a legitimate region for charge transfer to occur, the discontinuity, the truncated symmetry, and the concomitant impurity phases all affect the kinetics and thermodynamics of ion transport. By summarizing these studies, we aim to gain a better understanding about the manipulation of this key component at the atomic scale. It is noteworthy that due to different structural units and their arrangements, operating voltages, and electrolyte systems, the desirable interfaces and the corresponding surface engineering could vary remarkably from material to material. However, they are expected to share similar chemical/electrochemical properties such as high stability and fast charge transfer capability. Herein, several key conclusions have been made as follows, which may provide solutions to improve not only olivine, spinel, and layered oxides but, in broader terms, all intercalation host materials:

(a) Through surface modification, the poorly crystalline or disordered surface of cathode materials can be utilized for additional Li^+ binding sites, thus providing higher capacities.

(b) The ion transfer kinetics across the cathode/electrolyte interface can be tuned by choosing alternative solvents or surface doping, which could reconstruct the truncated surface symmetry and lower the migration energy barrier as well as the de-solvation energy, thus enabling better rate performance.

(c) To improve the rate capability of materials with poor electronic conductivity, surface depolarization of the cathode material can be achieved by a conductive coating layer (*e.g.*, carbon or conductive polymer), which is preferably in close (*e.g.*, molecular level) contact with the cathode surface.

(d) In order to stabilize the cycling performance of the cathode materials that are prone to surface degradation, chemically and electrochemically stable phases or a coating layer could be introduced to the outermost layer of the particle.

Conflicts of interest

There are no conflicts to declare.

Acknowledgements

This work is supported by National Key R&D Program of China (2016YFB0700600), National Natural Science Foundation of China (No. 51672012), Guangdong Key-Lab Project (No. 2017B0303010130), and Shenzhen Science and Technology Research Grant (ZDSYS20170728102618). KX also wants to thank the Joint Center for Energy Storage Research, an Energy Innovation Hub funded by the U.S. Department of Energy, Office of Science, Basic Energy Sciences through IAA SN2020957.

Notes and references

1 A. K. Padhi, K. S. Nanjundaswamy and J. B. Goodenough, *J. Electrochem. Soc.*, 1997, **144**, 1188–1194.
2 J. Zheng, Y. Ye and F. Pan, *Natl. Sci. Rev.*, 2019, **2**, 242–245.
3 X. Liu, Y. J. Wang, B. Barbiellini, H. Hafiz, S. Basak, J. Liu, T. Richardson, G. Shu, F. Chou, T. C. Weng, D. Nordlund, D. Sokaras, B. Moritz, T. P. Devereaux, R. Qiao, Y. De Chuang, A. Bansil, Z. Hussain and W. Yang, *Phys. Chem. Chem. Phys.*, 2015, **17**, 26369–26377.
4 J. Lu, Z. Chen, F. Pan, L. A. Curtiss and K. Amine, *Nat. Nanotechnol.*, 2016, **11**, 1031–1038.
5 J. Hu, H. Zeng, X. Chen, Z. Wang, H. Wang, R. Wang, L. Wu, Q. Huang, L. Kong, J. Zheng, Y. Xiao, W. Zhang and F. Pan, *J. Phys. Chem. Lett.*, 2019, 4794–4799.
6 J. Zheng, Y. Ye, T. Liu, Y. Xiao, C. Wang, F. Wang and F. Pan, *Acc. Chem. Res.*, 2019, **52**, 2201–2209.
7 B. Xiao and X. Sun, *Adv. Energy Mater.*, 2018, **8**, 1802057.
8 G. Xu, Z. Liu, C. Zhang, G. Cui and L. Chen, *J. Mater. Chem. A*, 2015, **3**, 4092–4123.
9 S. Kobayashi, C. A. J. Fisher, T. Kato, Y. Ukyo, T. Hirayama and Y. Ikuhara, *Nano Lett.*, 2016, **16**, 5409–5414.
10 G. K. P. Dathar, D. Sheppard, K. J. Stevenson and G. Henkelman, *Chem. Mater.*, 2011, **23**, 4032–4037.
11 S. K. Jung, H. Gwon, J. Hong, K. Y. Park, D. H. Seo, H. Kim, J. Hyun, W. Yang and K. Kang, *Adv. Energy Mater.*, 2014, **4**, 1300787.
12 B. Kang and G. Ceder, *Nature*, 2009, **458**, 190.
13 B. Lung-Hao, Hu, F. Y. Wu, C. Te Lin, A. N. Khlobystov and L. J. Li, *Nat. Commun.*, 2013, **4**, 1687.
14 Q. Zhao, Y. Zhang, Y. Meng, Y. Wang, J. Ou, Y. Guo and D. Xiao, *Nano Energy*, 2017, **34**, 408–420.
15 C. Lu, X. Jiang, W. Sun, Z. Wang, K. Sun, D. W. Rooney and J. Wang, *J. Mater. Chem. A*, 2017, **5**, 24636–24644.
16 Y. Duan, B. Zhang, J. Zheng, J. Hu, J. Wen, D. J. Miller, P. Yan, T. Liu, H. Guo, W. Li, X. Song, Z. Zhuo, C. Liu, H. Tang, R. Tan, Z. Chen, Y. Ren, Y. Lin, W. Yang, C. M. Wang, L. W. Wang, J. Lu, K. Amine and F. Pan, *Nano Lett.*, 2017, **17**, 6018–6026.
17 H. Wang, N. Zhao, C. Shi, L. Ma, F. He, C. He, J. Li and E. Liu, *Electrochim. Acta*, 2017, **247**, 1030–1037.
18 Y. Duan, L. Yang, M. J. Zhang, Z. Chen, J. Bai, K. Amine, F. Pan and F. Wang, *J. Mater. Chem. A*, 2019, **7**, 513–519.
19 M.-J. Zhang, X. Hu, M. Li, Y. Duan, L. Yang, C. Yin, M. Ge, X. Xiao, W.-K. Lee, J. Y. P. Ko, K. Amine, Z. Chen, Y. Zhu, E. Dooryhee, J. Bai, F. Pan and F. Wang, *Adv. Energy Mater.*, 2019, 1901915.
20 Z. Wu, S. Ji, J. Zheng, Z. Hu, S. Xiao, Y. Wei, Z. Zhuo, Y. Lin, W. Yang, K. Xu, K. Amine and F. Pan, *Nano Lett.*, 2015, **15**, 5590–5596.
21 Y. Li, H. Chen, K. Lim, H. D. Deng, J. Lim, D. Fraggedakis, P. M. Attia, S. C. Lee, N. Jin, J. Moškon, Z. Guan, W. E. Gent, J. Hong, Y. S. Yu, M. Gaberšček, M. S. Islam, M. Z. Bazant and W. C. Chueh, *Nat. Mater.*, 2018, **17**, 915–922.
22 J. Zheng, Y. Hou, Y. Duan, X. Song, Y. Wei, T. Liu, J. Hu, H. Guo, Z. Zhuo, L. Liu, Z. Chang, X. Wang, D. Zherebetskyy, Y. Fang, Y. Lin, K. Xu, L. W. Wang, Y. Wu and F. Pan, *Nano Lett.*, 2015, **15**, 6102–6109.
23 X. Song, T. Liu, J. Amine, Y. Duan, J. Zheng, Y. Lin and F. Pan, *Nano Energy*, 2017, **37**, 90–97.
24 W. Tang, X. Song, Y. Du, C. Peng, M. Lin, S. Xi, B. Tian, J. Zheng, Y. Wu, F. Pan and K. P. Loh, *J. Mater. Chem. A*, 2016, **4**, 4882–4892.
25 J. Hu, W. Li, Y. Duan, S. Cui, X. Song, Y. Liu, J. Zheng, Y. Lin and F. Pan, *Adv. Energy Mater.*, 2017, **7**, 1601894.
26 J. Hu, W. Ren, X. Chen, Y. Li, W. Huang, K. Yang, L. Yang, Y. Lin, J. Zheng and F. Pan, *Nano Energy*, 2020, **74**, 104864.
27 W. Zhang, X. Sun, Y. Tang, H. Xia, Y. Zeng, L. Qiao, Z. Zhu, Z. Lv, Y. Zhang, X. Ge, S. Xi, Z. Wang, Y. Du and X. Chen, *J. Am. Chem. Soc.*, 2019, **141**, 14038–14042.
28 P. Bai and M. Z. Bazant, *Nat. Commun.*, 2014, **5**, 3585.
29 H. Wang, R. Wang, L. Liu, S. Jiang, L. Ni, X. Bie, X. Yang, J. Hu, Z. Wang, H. Chen, L. Zhu, D. Zhang, Y. Wei, Z. Zhang, S. Qiu and F. Pan, *Nano Energy*, 2017, **39**, 346–354.
30 W. Ren, K. Wang, J. Yang, R. Tan, J. Hu, H. Guo, Y. Duan, J. Zheng, Y. Lin and F. Pan, *J. Power Sources*, 2016, **331**, 232–239.
31 Y. Liu, J. Liu, J. Wang, M. N. Banis, B. Xiao, A. Lushington, W. Xiao, R. Li, T. K. Sham, G. Liang and X. Sun, *Nat. Commun.*, 2018, **9**, 929.
32 D. Lepage, C. Michot, G. Liang, M. Gauthier and S. B. Schougaard, *Angew. Chem., Int. Ed.*, 2011, **50**, 6884–6887.
33 L. Guo, Y. Zhang, J. Wang, L. Ma, S. Ma, Y. Zhang, E. Wang, Y. Bi, D. Wang, W. C. McKee, Y. Xu, J. Chen, Q. Zhang, C. Nan, L. Gu, P. G. Bruce and Z. Peng, *Nat. Commun.*, 2015, **6**, 7898.
34 K. S. Park, P. Xiao, S. Y. Kim, A. Dylla, Y. M. Choi, G. Henkelman, K. J. Stevenson and J. B. Goodenough, *Chem. Mater.*, 2012, **24**, 3212–3218.
35 Y. Li, Y. Zhang, J. Ma, L. Yang, X. Li, E. Zhao, S. Fan, G. Xu, S. Yang and C. Yang, *J. Electrochem. Soc.*, 2019, **166**, A410–A415.
36 Z. Wu, X. Han, J. Zheng, Y. Wei, R. Qiao, F. Shen, J. Dai, L. Hu, K. Xu, Y. Lin, W. Yang and F. Pan, *Nano Lett.*, 2014, **14**, 4700–4706.
37 D. Aurbach, B. Markovsky, G. Salitra, E. Markevich, Y. Talyossef, M. Koltypin, L. Nazar, B. Ellis and D. Kovacheva, *J. Power Sources*, 2007, **165**, 491–499.
38 J. Wang, Y. Tang, J. Yang, R. Li, G. Liang and X. Sun, *J. Power Sources*, 2013, **238**, 454–463.
39 W. Huang, J. Hu, L. Yang, W. Zhao, Z. Wang, H. Wang, Z. Guo, Y. Li, J. Liu, K. Yang and F. Pan, *ACS Appl. Mater. Interfaces*, 2019, **11**, 957–962.

40 T. Liu, A. Dai, J. Lu, Y. Yuan, Y. Xiao, L. Yu, M. Li, J. Gim, L. Ma, J. Liu, C. Zhan, L. Li, J. Zheng, Y. Ren, T. Wu, R. Shahbazian-Yassar, J. Wen, F. Pan and K. Amine, *Nat. Commun.*, 2019, **10**, 1–11.
41 Y. Wu, L. Ben, H. Yu, W. Qi, Y. Zhan, W. Zhao and X. Huang, *ACS Appl. Mater. Interfaces*, 2019, **11**, 6937–6947.
42 P. Yan, J. Zheng, J. Liu, B. Wang, X. Cheng, Y. Zhang, X. Sun, C. Wang and J. G. Zhang, *Nat. Energy*, 2018, **3**, 600–605.
43 G. L. Xu, Q. Liu, K. K. S. Lau, Y. Liu, X. Liu, H. Gao, X. Zhou, M. Zhuang, Y. Ren, J. Li, M. Shao, M. Ouyang, F. Pan, Z. Chen, K. Amine and G. Chen, *Nat. Energy*, 2019, **4**, 484–494.
44 L. Yang, Y. Xia, L. Qin, G. Yuan, B. Qiu, J. Shi and Z. Liu, *J. Power Sources*, 2016, **304**, 293–300.
45 Y. K. Sun, Z. Chen, H. J. Noh, D. J. Lee, H. G. Jung, Y. Ren, S. Wang, C. S. Yoon, S. T. Myung and K. Amine, *Nat. Mater.*, 2012, **11**, 942–947.
46 D. Kong, J. Hu, Z. Chen, K. Song, C. Li, M. Weng, M. Li, R. Wang, T. Liu, J. Liu, M.-J. Zhang, Y. Xiao and F. Pan, *Adv. Energy Mater.*, 2019, 1901756.
47 Q. Wei, X. Wang, X. Yang, B. Ju, B. Hu, H. Shu, W. Wen, M. Zhou, Y. Song, H. Wu and H. Hu, *J. Mater. Chem. A*, 2013, **1**, 4010–4016.
48 S. M. Oh, S. T. Myung, J. B. Park, B. Scrosati, K. Amine and Y. K. Sun, *Angew. Chem., Int. Ed.*, 2012, **51**, 1853–1856.
49 K. J. Kreder and A. Manthiram, *ACS Energy Lett.*, 2017, **2**, 64–69.
50 Z. Wu, S. Ji, T. Liu, Y. Duan, S. Xiao, Y. Lin, K. Xu and F. Pan, *Nano Lett.*, 2016, **16**, 6357–6363.

